The American Journal of Human Genetics, Volume *88*

Supplemental Data

Excess of De Novo Deleterious Mutations in Genes Associated with Glutamatergic Systems in Nonsyndromic Intellectual Disability

Fadi F. Hamdan, Julie Gauthier, Yoichi Araki, Da-Ting Lin, Yuhki Yoshizawa, Kyohei Higashi, A-reum Park, Dan Spiegelman, Sylvia Dobrzeniecka, Amélie Piton, Hideyuki Tomitori, Hussein Daoud, Christine Massicotte, Edouard Henrion, Ousmane Diallo, S2D group, Masoud Shekarabi, Claude Marineau, Michael Shevell, Bruno Maranda, Grant Mitchell, Amélie Nadeau, Guy D'Anjou, Michel Vanasse, Myriam Srour, Ronald G. Lafrenière, Pierre Drapeau, Jean Claude Lacaille, Eunjoon Kim, Jae-Ran Lee, Kazuei Igarashi, Richard L. Huganir, Guy A. Rouleau, and Jacques L. Michaud

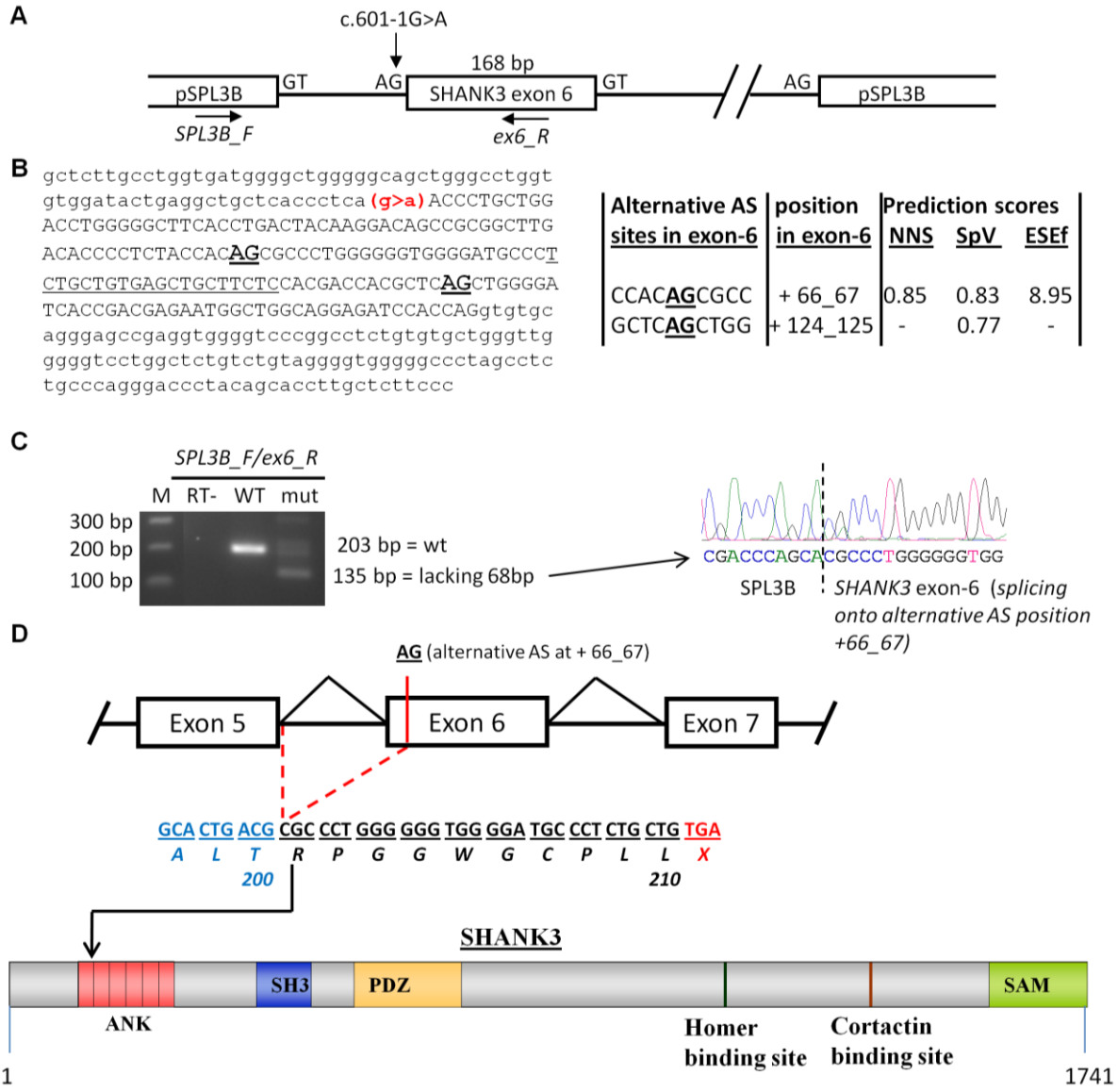

Figure S1. Exon-Trapping analysis of the splicing alteration caused by c.601-1G>A in *SHANK3*

Due to the unavailability of lymphoblastoid cell lines or additional blood samples for RNA extraction from the patient with the *SHANK3* heterozygous c.601-1G>A mutation, we employed a well utilized exon-trapping strategy to generate mRNA from transfected COS7 cells.

(A) Schematic representation of the *SHANK3* exon-6 trapping constructs in pSPL3B (Invitrogen); forward (SPL3B_F) and reverse (ex6_R) primers used for PCR are shown.

(B) Nucleotide sequence of *SHANK3* genomic DNA containing exon-6 (capital letters) and flanking intronic (small caps) sequences which were cloned from the patient's genomic DNA, as wild type (WT; amplified from the normal allele) or mutant (c.601-1G>A) (Mut; amplified from the mutant allele), in pSPL3B. The sequence of the reverse primer, ex6_R, is underlined; the splicing c.601-1G>A mutation at the splice acceptor site is highlighted in red (g>a). The 2 predicted alternative cryptic splice acceptor sites in exon-6 are underlined and bolded. Prediction scores for these alternative acceptor sites (AS) were according to three different programs: nnsplice 0.9 (NNS; http://www.fruitfly.org/seq_tools/splice.html), SpliceView (SpV;

http://bioinfo.itb.cnr.it/oriel/splice-view.html), and ESEfinder (ESEf; http://rulai.cshl.edu/cgi-bin/tools/ESE3/esefinder.cgi?process=home).
(C) COS-7 cells were transfected using Lipofectamine 2000 (Invitrogen) with either WT or Mut pSPL3B-SHANK3-exon-6 plasmids and the cells were harvested after 48 hrs, and total RNAs were extracted using the TRIzol reagent (Invitrogen). First strand cDNAs were synthesized from 1 μg of total RNA of each sample using random hexamers and MMLV reverse transcriptase (Invitrogen). The generated cDNAs were amplified with a forward pSPL3 vector-specific primer (SPL3B_F: 5'-CTGAGTCACCTGGACAACC-3') and a reverse primer located in exon-6 of SHANK3 (ex6_R: 5'-GAGAAGCAGCTCACAGCAGA-3'). The PCR products were resolved on a 2% agarose gel, purified, and then sequenced using the pSPL3 vector-specific primers. A negative control containing Mut total RNA without reverse transcription (RT-) was included. A 203 bp PCR product was obtained from the WT sample, corresponding to the properly spliced SHANK3-exon 6 sequence, and a predominant 135 bp product was obtained from the Mut sample. DNA sequencing of this 135 bp showed that it corresponded to the use of the first alternative splice acceptor "ag" site at positions +66_67 in exon-6. The chromatogram displaying the mutant cDNA sequence at the junction SPL3B/SHANK3-exon-6 is shown.
(D) Schematic representation of exons 5, 6 and 7 of *SHANK3* with wild-type (black) and mutant (red) splicing. The c.601-1G>A mutation abolishes the normal acceptor site and leads to the utilization of a cryptic acceptor site located at +66_67 in exon-6. This results in a frameshift and a premature stop codon at position 211. The position of the resulting frameshift with respect to known functional domains of SHANK3 is shown in the bottom panel.

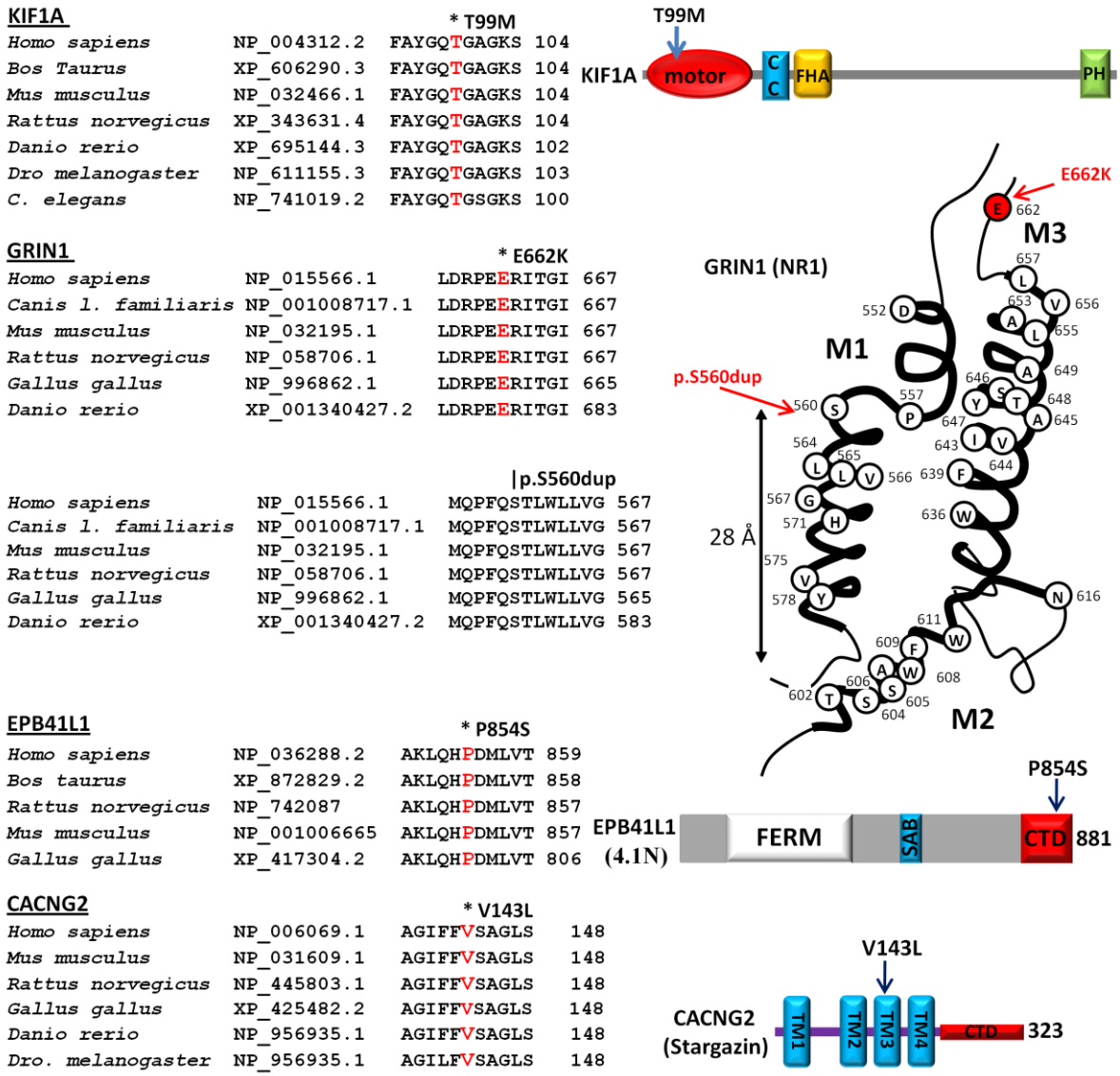

Figure S2. Amino acid conservation of the residues affected with missense DNMs

Left panels: Amino acid alignments were generated using homologene (NCBI) and the amino acid sequences flanking the various DNMs are shown, along with the corresponding accession number for each protein sequence. Right panels, the identified DNMs are localized on the predicted structural representations of each of the implicated genes. Various important protein domains are indicated for each protein: For KIF1A, motor domain (pos. 3-361), coiled coil domain (CC; pos. 429-462), fork head-associated domain (FHA; pos. 516-572), pleckstrin homology domain (PH; 1575-1673); for GRIN1, M1-M3 represent transmembrane domain regions of the receptor's channel pore (M1, pos. 560-579; M2, pos. 601-613; M3, pos. 627-657); for EPB41L1 (4.1N), FERM domain (pos. 97-378), spectrin-actin-binding (SAB, pos. 483-541) domain, and a C-terminal domain (CTD, binds AMPARs; pos. 746-881); for CACNG2 (Stargazin), transmembrane 1-4 (TM1, pos. 10-30; TM2, pos. 104-124; TM3, pos. 134-154; TM4, pos. 182-202), and a C-terminal domain (CTD, pos, ~ 210-323, binds AMPARs).

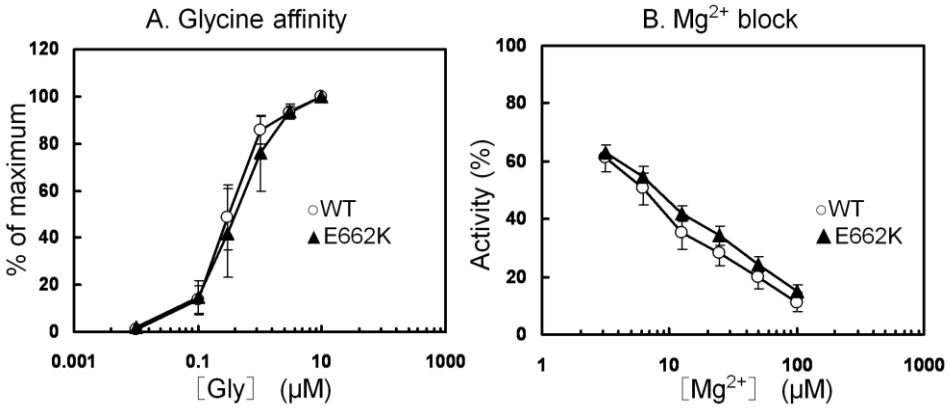

Figure S3. Effect of p.Glu662Lys mutation on NR1's affinity to glycine and its response in presence of Mg^{2+}

Xenopus laevis oocytes were co-injected with NR1 (WT or E662K) and NR2B complementary RNAs and macroscopic current were recorded as described in supplementary methods.

(A) Glycine affinity. Currents were measured at -20 mV in the presence of 10 mM Glu and various concentrations of Gly shown in the figure. Currents obtained with 10 mM Gly were expressed as 100 %.

(B) Mg^{2+} block. Glu+Gly-activated currents were measured at -100 mV in the presence of various concentrations of Mg^{2+}. Currents obtained without Mg^{2+} were expressed as 100 %.

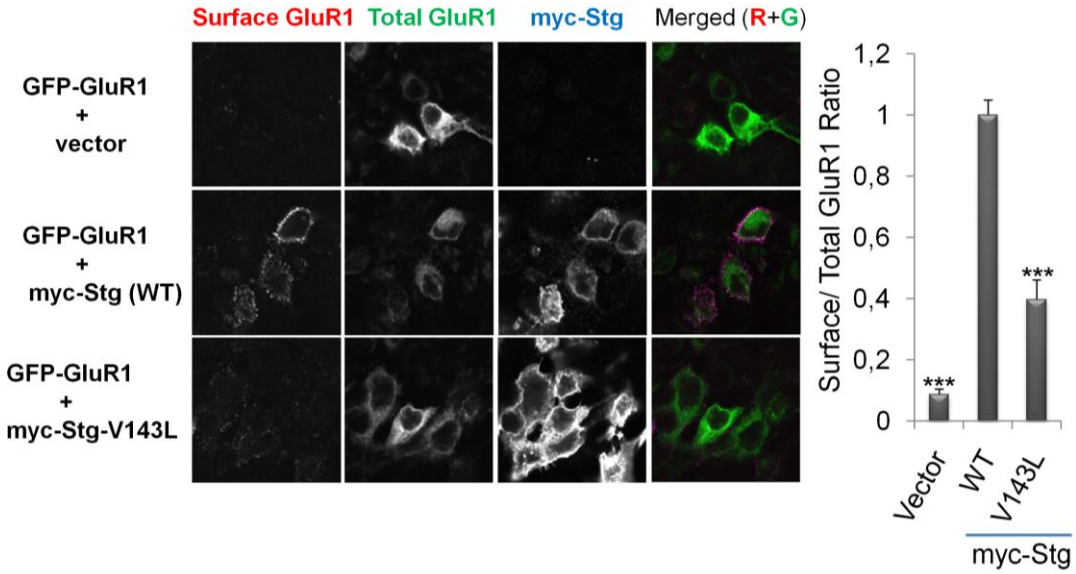

Figure S4. Effect of p.Val143Leu mutation on AMPAR GluR1 surface expression in transfected HEK293 cells

(A) HEK293 cells were co-transfected with GFP-GluR1 and indicated Stargazin (myc-Stg) constructs and stained with anti-GFP (to detect surface R1) in a non-permeabilized condition. Co-expression of myc-stg with GluR1 in HEK293 cells greatly increases surface expression of GFP-GluR1, in contrast to cotransfections with the V143L-Stg mutant which has reduced ability to bring GluR1 to plasma membrane.

(B) Quantification of staining results (mean ± SE, n=4,*** $p<0.001$ One-way ANOVA followed by Tukey post-hoc test)

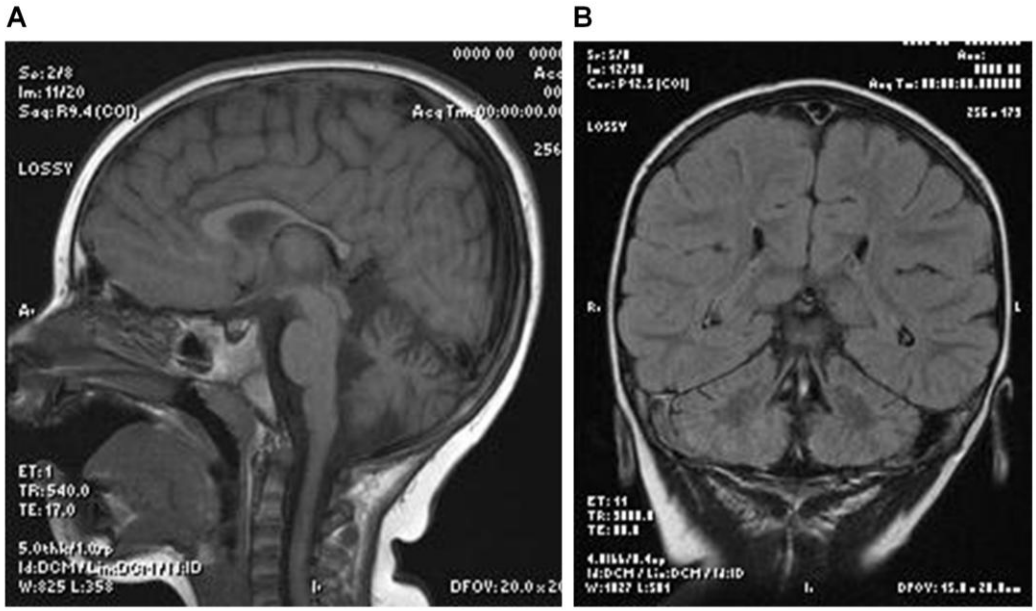

Figure S5. Brain MRI for the patient with the p.Thr99Met KIF1A DNM
(A) Sagittal T1 MR image showing mild atrophy of vermis.
(B) Coronal T2 MR image showing discrete atrophy of the cerebellar hemispheres.

Tables S1-S5.
(See accompanying Excel spreadsheet.)